COMPLEX SYSTEM MODELING AND SIMULATION
ISSN 2096-9929 03/06 pp 118−128
Volume 3, Number 2, June 2023
DOI: 10.23919/CSMS.2023.0004

Modeling Common-Mode Current Due to Asymmetric Aging of Machine Winding Insulation

Jin Zhao* and Aaron D. Brovont

Abstract: Machine stator winding insulation degradation is one of the main results of machine aging. It is non-negligible once this degradation process becomes asymmetric between phases. The traditional way to determine the insulation state of health is a partial discharge test. However, this method requires the system offline, which causes production loss and extra administrative burden. This paper presents an idea for better characterizing the insulation machine's state of health using common-mode (CM) behavior in the machine-drive system. With the help of circuit decomposition methods and modeling tools, the CM quantities due to asymmetric aging show a unique characteristic that distinguishes itself from other differential-mode (DM) quantities in the equivalent circuit. It is shown effective to represent the asymmetric aging effect from the detection of system leakage current. This paper provides an analytical method to quantify this characteristic from mathematical approaches, and a proper approximation has been made on the CM equivalent model (CEM) such that the CM behavior is accurately characterized. The proposed method will serve the purpose of predicting machine abnormal behavior using the simple RLC circuit. Researchers can adapt this method to quantify and characterize the machine insulation state of health (SOH).

Key words: common-mode; equivalent circuit; machine decomposition; machine stator winding; insulation health; model approximation

1 Introduction

Since the widespread adoption of pulse-width modulation (PWM) based electric drive systems, one of the major causes of machine failure is the degradation of the stator winding insulation[1−3]. For this reason, it is common to conduct a battery of tests (e.g., insulation resistance, capacitance, partial discharge, etc.) to estimate a critical machine's insulation state of health (SOH) whenever it is offline and available[4, 5]. However, such offline diagnosis is typically opportunistic and infrequent. It provides poor temporal resolution, and therefore, the insulation health data obtained by offline tests often have little predictive value. To overcome this fault, a growing body of literature is devoted to online monitoring of machine insulation SOH[5−12].

A trending method of non-invasive machine winding insulation monitoring is to apply high-frequency (HF) switching oscillation to the gate drive[13, 14]. This is done by installing a coil-based sensor into the machine winding and executing measurement during idle or before machine startup. In this way it prevents the external HF excitation from being introduced into the machine. The common-mode (CM) current profile of the machine is then derived from measuring the series and parallel resonance frequency responses. In Refs. [15, 16], switch oscillation current is also used to create a mathematical model for characterizing HF transient ground-wall insulation status. Such a method yields a

• Jin Zhao is with the Department of Electrical and Computer Engineering, The University of Alabama, Tuscaloosa, AL 35487, USA. E-mail: jzhao95@ieee.org.
• Aaron D. Brovont is with the PC Krause and Associates, West Lafayette, IN 47906, USA. E-mail: abrovont@pcka.com.
* To whom correspondence should be addressed.
※ This article was recommended by Associate Editor Hua Geng.
Manuscript received: 2022-09-26; revised: 2023-01-16; accepted: 2023-02-26

decent result on SOH monitoring, yet the monitoring and detection can only be at a discrete manner, which only serves a limited function in predicting the machine insulation degradation process. In addition, while implementing, machine downtime is still required, and the oscillation is aside from normal operation, which is unattainable for continuous monitoring purposes.

Other machine insulation fault diagnosis means are also popular among different research applications. Dielectric frequency response analysis applies a high-frequency voltage to the windings and measures the dynamic response of insulation[17, 18]. The current signature analysis involves analyzing the current flowing through the machine windings to identify changes or abnormalities that may indicate a problem with the insulation, without physically accessing the windings[19–21]. CM circuit analysis is also popular in monitoring the state of health of electric machine insulation. It involves analyzing the CM currents and voltages in the machine windings to identify abnormalities or changes that may indicate a problem with the insulation. CM behavior has been considered as an interesting aspect in quantifying machine winding insulation SOH. In Ref. [22], an illustrative CM model is proposed; in Ref. [23], the single-phase aging effect is characterized in the phasor diagram, showing that the leakage impedance changes with accelerated thermal stress on insulation material; in Ref. [11], a simplified machine model is presented with insulation leakage parasitic to ground. However, none of those models showed an insightful observation of how CM behavior can be related to the insulation SOH. In addition, the accelerated thermal stress forces the insulation material to degrade in a rapid fashion so that the CM behavior is obviously perceivable. On the contrary, in actual events, the degradation should be a gradual process so the change in CM current is trivial considering it is a relatively short period of time. In order to characterize the small change in CM current, the CM modeling technique is a useful tool to provide a straightforward observation of the insulation SOH in the real-time event.

The variation in mutual inductance of an electric machine can also contribute to CM behavior and affect machine performance. However, since it is a measure of the inductive coupling between two separate windings, whereas the health of insulation is primarily related to its ability to insulate electrically and withstand the electrical and mechanical stresses of operation, therefore mutual inductance does not provide information about the SOH condition of the insulation. It does not change with the insulation aging process. However, mutual inductance can be used in certain applications such as detecting the presence of inter-turn short-circuits in the winding, but it is not commonly used for characterizing the health of the insulation.

A typical electric machine-drive system may be modeled as represented in Fig. 1. The machine is controlled by an ideal two-level, three-phase inverter supplied by a well-conditioned dc bus. The inductance of the feeder cables and the first few turns of the stator winding is represented by L_f and its equivalent series resistance (ESR) is R_f. The insulation leakage path is placed after the first few turns of the stator winding of each phase. The leakage impedance can be represented

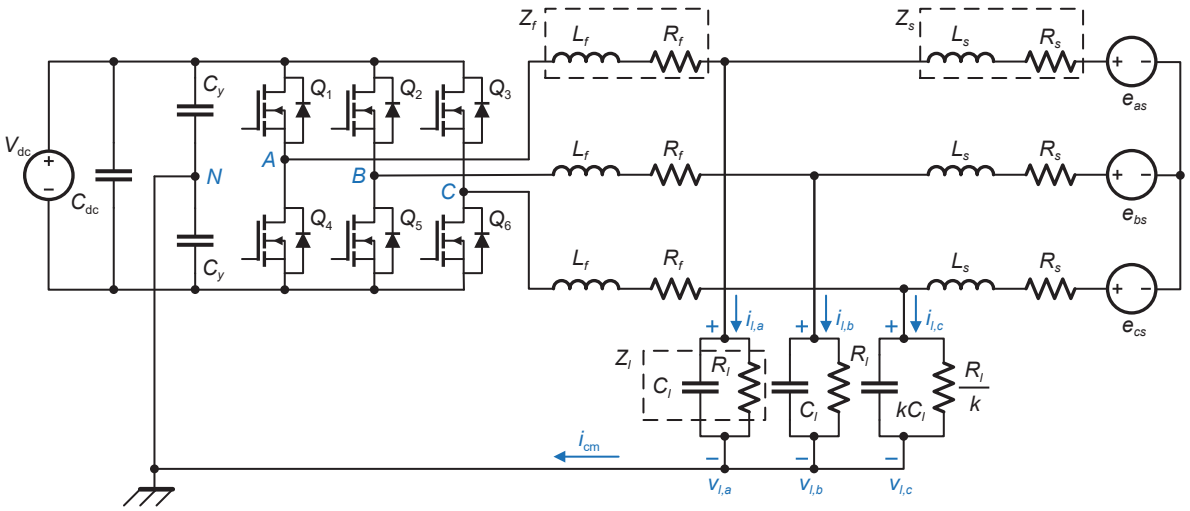

Fig. 1 Simplified machine-drive system with leakage parasitics.

as a parallel resistor and capacitor[4, 22]. Beyond the leakage path, the remainder of the stator windings consists of stator inductance L_s, stator resistance R_s, and the back-electromotive force (EMF) e_{xs}, where $x \in \{a, b, c\}$. This particular part of the stator winding at each phase represents the high-frequency component in the machine system, where no CM returning path is formed due to the symmetric layout. The back-EMF in the model is represented as a set of balanced voltage sources.

It is noted that when the machine-drive system is perfectly balanced, no leakage currents are expected to pass through the leakage path, thus the CM leakage current $i_{\text{cm}} = 0$. At the earliest stage of a machine, the aging effects are negligible since the system components are formed with high uniformity. After a certain amount of time of operation, the aging effects start to step in such as reduced capacity and increased operating temperatures/noises. While on the power electronics point of view, such responses can be the result of increased rotor time constant and changing rotor/winding impedance. The behavior of an electric machine due to asymmetric aging can differ among different parameters. For example, bearing wear can lead to increased friction; and rotor core degradation can lead to decreased flux linkage and reduced performance. Parameters such as torques, slip, terminal voltage, etc. could result in prominent and acute effects such as unstable power output, voltage or current surge, and abrupt machine operation failure. On the other hand, machine winding insulation asymmetry is a gradual process that can be recognized from a continuous observation. To be specific, having asymmetric aging of the machine winding insulation can lead to a number of issues:

- **Increased risk of electrical failure:** If the insulation on one phase of winding has aged more than the other phases, it may be more prone to electrical breakdown. This can lead to an increased risk of electrical failure and potential damage to the machine.
- **Decreased performance:** An asymmetrically aged winding may not operate as efficiently as a symmetrically aged winding.
- **Increased heat generation and vibration:** Asymmetric aged winding may generate more heat during operation, which can be a sign of increased resistance and reduced efficiency. Such changes in electrical parameters would also lead to increased vibration, which can impact the performance of the machine.

It is important to regularly monitor and test electric machines to identify any signs of asymmetric aging and take appropriate action to address any issues that are found. In addition to these visual and operational signs, the machine may also be tested using specialized equipment, such as oscilloscopes or transient recorders, to more accurately assess its condition.

By introducing the leakage path to the machine winding, the asymmetric behavior that exhibits CM quantities will be captured and analyzed to determine the current SOH of the machine. This paper is mainly focusing on the CM behavior characterization due to asymmetry on the leakage parasitics, while the high-frequency component and its effect in the stator winding are therefore out of concern.

Without loss of generality, the parameter k in Fig. 1 is defined as the admittance factor on one of the three phases, in order to create a single-phase-aging scenario. It is assumed for sake of analysis that phase C is aging at a faster rate than phases A and B. It is further assumed that phases A and B will be aging at an approximately equal rate in the proposed model. The CM leakage current i_{cm} in this mixed-mode (MM) circuit flows through the leakage impedance and travels back to the neutral point N on the dc side, then goes back into the neutral-formed capacitors C_y connecting the upper and lower rails of the drive-side of the system.

The admittance asymmetry factor k introduced in Fig. 1 is a time-dependent variable representing the insulation degradation over time, ideally $k = 1$, and all three phases age at the same rate. Related research on machine aging has shown that the winding insulation impedance is changing under both thermal and electrical stresses in a fashion that before a certain operating point, the leakage capacitance C_l decreases while simultaneously the parallel resistance R_l increases[4, 5], which means k is increasing in this stage in the proposed MM model. After this stage, C_l will roughly maintain at a relatively small value and the material resin starts to lose weight, thermal stress becomes the dominant effect in the aging process until the machine failure occurs[24, 25]. Hence, the change of k results in the variation of CM quantities on the leakage path, which could be useful in monitoring the insulation degradation rate in the machine-drive system via observing CM behavior in the decomposed equivalent circuit. Furthermore, with proper

approximations, this CM behavior can be emulated within a simplified RLC circuit driven by an ideal ac voltage source, which will be mentioned in detail in Section 4.

In the remainder of this paper, Section 2 applies a mathematical modeling approach in decomposing machine-drive system model into differential-mode (DM) and CM equivalent models (DEM, CEM), in order to characterize the CM behavior on the leakage path. Section 3 gives the model validation between MM and decomposed models as well as system operational parameters and simulation environments. Section 4 introduces a feasible circuit approximation such that the CM quantities in the MM model can be precisely predicted with a simple RLC circuit driven by an ideal ac source. Section 5 discusses the modeling and approximation techniques related with insulation SOH monitoring in practical use. In conclusion, the modeling and approximating techniques presented in this paper should be able to provide an insightful tool for online monitoring of machine stator winding insulation health.

2 Modal Decomposition of the Machine-Drive System with Leakage Parasitics

From the proposed model in Fig. 1, the decomposition work can be done in two steps: (1) decompose the machine-drive system considering all the components are balanced or symmetric, and (2) introduce the asymmetric leakage parasitic parameters into the system. The first step can be done by inspection, as shown in Fig. 2, where Fig. 2a is the phase *A* to *B* DM decomposed model or namely DEM-AB, and Fig. 2b is DEM-BC. It is noted that since all the circuit elements are perfectly symmetric with respect to positive/ negative rails (on dc-side) and phases (on ac-side), there are no leakage currents exhibited in any part of the system. In other words, CEM does not exist at this point. The differential dc bus voltage is defined as

$$v_{s,ab}^{\mathrm{dm}} \triangleq v_{Q_2} - v_{Q_1} = v_{Q_4} - v_{Q_5} = (q_1 - q_2)V_{\mathrm{dc}} \tag{1}$$

$$v_{s,bc}^{\mathrm{dm}} \triangleq v_{Q_3} - v_{Q_2} = v_{Q_5} - v_{Q_6} = (q_2 - q_3)V_{\mathrm{dc}} \tag{2}$$

where v_{Qx} is the gate voltage depending on the switch position q_x

$$q_x = \begin{cases} 0, \text{ closed;} \\ 1, \text{ open} \end{cases} \tag{3}$$

where $x \in \{1, 2, ..., 6\}$. Since the system is symmetric, the differential back-EMF only provides phase-gain, while magnitude-gain equals zero. Consequentially, impedance adds in series from DM point of view.

In order to properly model the insulation leakage impedance in Fig. 1, when $k \neq 1$, the phase *C* leakage branch becomes asymmetric which introduces mode-conversion between the DM and CM behaviors of the system. Since k is defined as the admittance factor, the leakage impedance Z_l (or equivalently, leakage admittance Y_l) of each phase can be expressed as

$$Z_l = R_l \,//\, \frac{1}{\mathrm{j}\omega C_l} \tag{4}$$

$$Y_l = \frac{1}{Z_l} = \frac{1}{R_l} + \mathrm{j}\omega C_l \tag{5}$$

For the leakage current, by definition

$$\begin{bmatrix} i_{l,a} \\ i_{l,b} \\ i_{l,c} \end{bmatrix} = Y_l \begin{bmatrix} 1 & 0 & 0 \\ 0 & 1 & 0 \\ 0 & 0 & k \end{bmatrix} \begin{bmatrix} v_{l,a} \\ v_{l,b} \\ v_{l,c} \end{bmatrix} \tag{6}$$

where $i_{l,x}$ and $v_{l,x}$ are defined as the leakage currents and voltage drops on each phase, respectively, $x \in \{a, b, c\}$. Following the same decomposition procedure detailed in Ref. [26], the decomposed DM and CM current identity is shown in Eq. (7),

$$\begin{bmatrix} i_{l,ab}^{\mathrm{dm}} \\ i_{l,bc}^{\mathrm{dm}} \\ i_{l}^{\mathrm{cm}} \end{bmatrix} = Y_l \cdot \overbrace{\begin{bmatrix} \frac{1}{2} & 0 & 0 \\ \frac{k-1}{6} & \frac{2k+1}{6} & \frac{1-k}{2} \\ \frac{1-k}{3} & \frac{2(1-k)}{3} & k+2 \end{bmatrix}}^{\boldsymbol{K}_y} \begin{bmatrix} v_{l,ab}^{\mathrm{dm}} \\ v_{l,bc}^{\mathrm{dm}} \\ v_{l}^{\mathrm{cm}} \end{bmatrix} \tag{7}$$

where $\boldsymbol{K}_y$ is defined as the mode-conversion admittance matrix. Since DM quantities are always defined between two phases at a time, the decomposed leakage current matrix is formed with two DM currents and one CM current. In addition, it is by design that between

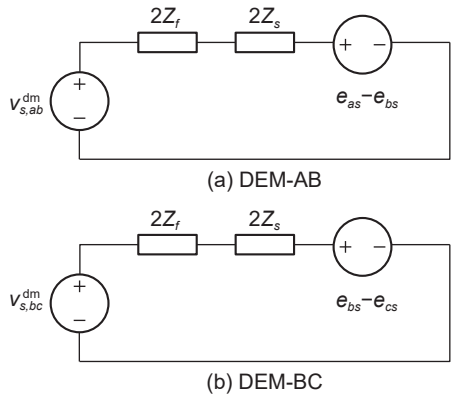

Fig. 2 DEM-AB and DEM-BC of the machine-drive system without leakage parasitics.

phases A and B, all the parameters are perfectly balanced. This results in no induced CM current, therefore also no mode-conversion terms. From Eq. (7), the leakage currents in DM and CM forms can be expressed as

$$v_{l,ab}^{\mathrm{dm}} = 2Z_l \cdot i_{l,ab}^{\mathrm{dm}} \tag{8}$$

$$v_{l,bc}^{\mathrm{dm}} = \frac{6}{2k+1} Z_l \cdot i_{l,bc}^{\mathrm{dm}} + \overbrace{\left[-\frac{k-1}{2k+1} v_{l,ab}^{\mathrm{dm}} - \frac{3(1-k)}{2k+1} v_l^{\mathrm{cm}} \right]}^{\triangleq v_{l,bc}^{\mathrm{cm}\to\mathrm{dm}}} \tag{9}$$

$$v_l^{\mathrm{cm}} = \frac{1}{k+2} Z_l \cdot i_l^{\mathrm{cm}} + \overbrace{\left[-\frac{1}{3} \cdot \frac{1-k}{k+2} v_{l,ab}^{\mathrm{dm}} - \frac{2}{3} \cdot \frac{1-k}{k+2} v_{l,bc}^{\mathrm{dm}} \right]}^{\triangleq v_l^{\mathrm{dm}\to\mathrm{cm}}} \tag{10}$$

where $v_{l,bc}^{\mathrm{cm}\to\mathrm{dm}}$ in Eq. (9) is defined as the CM-to-DM mode-conversion voltage contributing to DEM-BC and $v_l^{\mathrm{dm}\to\mathrm{cm}}$ in Eq. (10) is defined as the DM-to-CM mode-conversion voltage contributing to CEM.

The overall decomposed models introduced by the above equations are shown in Fig. 3. The expressions of input voltage sources are shown in Eqs. (1), (2), and (11), respectively. The equivalent CM and DM impedance are defined as in Eqs. (12)–(14). Note that the dependent voltage source $v_{l,bc}^{\mathrm{cm}\to\mathrm{dm}}$ is the mode-conversion term in DEM-BC, which depends on the voltage drops across the leakage paths in both DEM-AB and CEM. Similarly, the mode-conversion term $v_l^{\mathrm{dm}\to\mathrm{cm}}$ in CEM also depends on both $v_{l,ab}^{\mathrm{dm}}$ and $v_{l,bc}^{\mathrm{dm}}$.

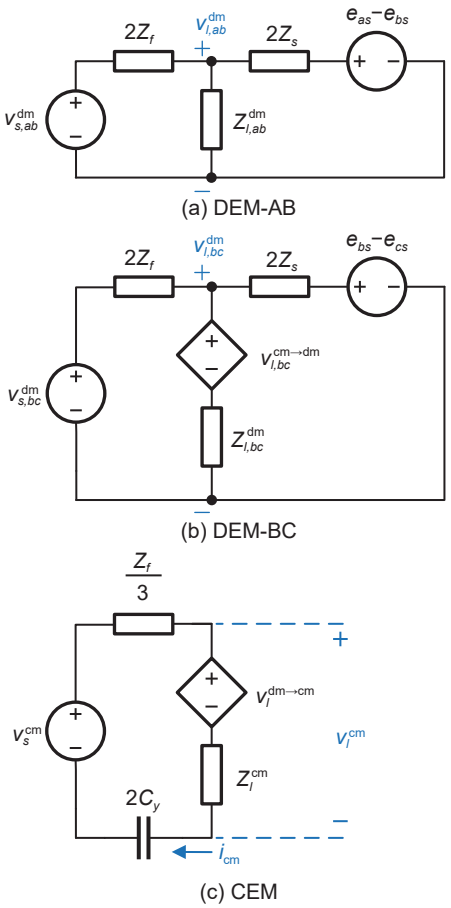

Fig. 3 Coupled DEM-AB, DEM-BC, and CEM of the overall machine-drive system.

$$v_s^{\mathrm{cm}} = \left[\frac{1}{3}(q_1 + q_2 + q_3) - \frac{1}{2} \right] V_{\mathrm{dc}} \tag{11}$$

$$Z_{l,ab}^{\mathrm{dm}} = 2Z_l \tag{12}$$

$$Z_{l,bc}^{\mathrm{dm}} = \frac{6}{2k+1} Z_l \tag{13}$$

$$Z_l^{\mathrm{cm}} = \frac{1}{k+2} Z_l \tag{14}$$

3 Model Validation and Parameters

The machine-drive model as well as the decomposed DEMs and CEM is implemented and simulated in MATLAB ver. 2022b with ASMG for Simulink Toolbox[27]. The operating system for simulation and analysis is MacOS Monterey ver. 12.6 with an Intel Core i5 processor at 2.9 GHz, and the installed RAM size is 8 GB. The machine winding and leakage parameters are acquired from the characterization of the experimental three-phase permanent magnet synchronous machine, and the operational parameters of the drive system are from the custom-designed medium-voltage testbed. Details of the parameters are shown in Table 1. Note that since this is a modeling approach in demonstrating the non-invasive method for CM leakage current characterization, without loss of generality, the parameters used in this paper are approximated.

Table 1 Machine-drive system parameters.

Parameter	Description	Value	Unit
V_{dc}	dc bus voltage	480	V
f_{sw}	Switching frequency	60	kHz
f_{o}	Fundamental frequency	60	Hz
C_{dc}	dc bus capacitance	500	μF
C_y	EMI filter capacitance	200	μF
L_f	First few turns of stator winding	20	mH
R_f	ESR of L_f	5	Ω
L_s	Remainder of stator windings	200	mH
R_s	ESR of L_s	50	Ω
C_l	Leakage capacitance	300	nF
R_l	Leakage resistance	5	kΩ

For a more accurate observation, the model relative tolerance is set at 10^{-8} which is two orders of magnitude less than the switching period. At $k = 10$, the leakage current comparison between MM model and the decomposed model is shown in Fig. 4. A strong match of i_{cm} between the MM model and the CEM is observed, indicating that the decomposed models represented in Fig. 3 are able to fully represent the CM and DM behaviors distinctively from the original MM machine-drive system.

Previous works on the insulation SOH monitoring are mostly performed offline[28–30], but the machine health should be continuously assessed and trended in real-time. The treatment of CM quantity in power electronics is often using shielding, chokes, or filters[31]; here on the contrary CM behavior is providing a new perspective in understanding the system with insulation asymmetric aging effects. The admittance factor k is designed in a way that the impedance angle of the leakage parasitic will not change before a certain degradation point[5]. While maintaining the asymmetric layout on the leakage path, maneuvering k results in a changing sinusoidal waveform of CM current, under the fixed fundamental frequency. Thus further analysis can be done focusing on the distribution of leakage impedance instead of single-phase degradation with the other two phases intact. Therefore, the purpose of the decomposition method presented in Section 2 is for a comprehensive understanding of CM and DM quantities in the machine model. Using the presented technique, the machine winding insulation SOH could be characterized and in addition failures of the machine could be predicted.

4 Analysis of Winding Asymmetry on CM Current

The CEM presented in Fig. 3c is able to characterize the transient and steady-state behavior of CM current in the machine-drive system for single-phase asymmetric aging. As mentioned in Section 1, k is the admittance factor that is intended to represent the machine insulation degradation. Since k ranges up and down throughout the entire machine lifespan, here let k sweep through the range $[0.1, 10]$ in order to validate the accuracy of the decomposed model. The steady-state behavior of CM current in Fig. 5 shows the features of amplitude change and phase shift in CM current under the same fundamental frequency. Figure 5 also indicates that single-phase aging effects represented by a varying k are perceptible in the CM perspective. When $k = 1$, the leakage paths become symmetric, and the amplitude of i_{cm} drops down to the minimum as the fundamental frequency component vanishes.

The decomposed CEM in Fig. 3c may be further simplified under reasonable assumptions with respect to k and i_{cm}. Specifically, an approximated CEM is created to represent the steady-state behavior of CM current in the asymmetric aging scenario by neglecting the high-frequency component from the machine-drive

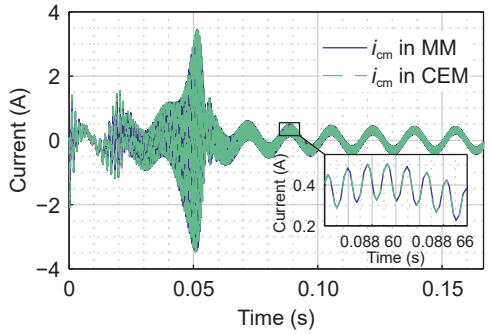

Fig. 4 CM current predicted by MM and decomposed models when $k = 10$.

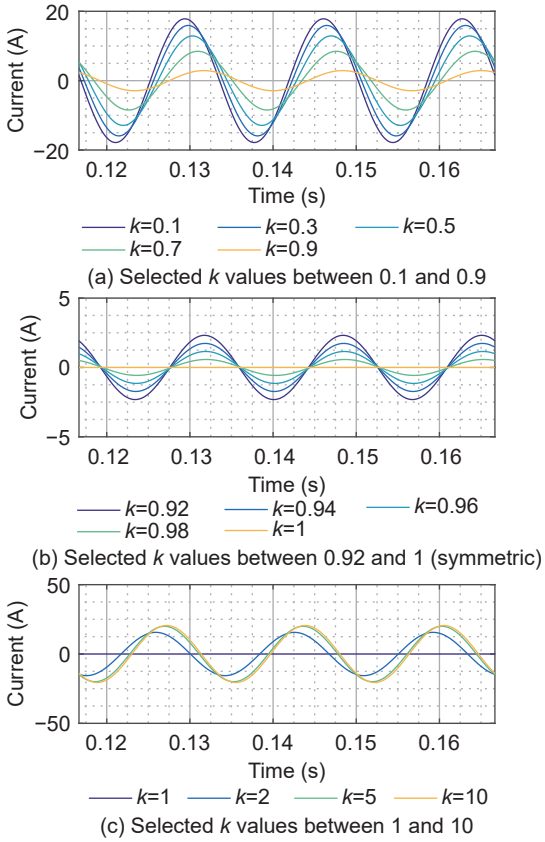

Fig. 5 CM current behavior under different values of admittance factor k.

system and approximating the mode-conversion voltage sources based on steady-state DM operation behavior. According to the definition of k, it is reasonable to ask that how asymmetry in the leakage path will affect the CM behavior in the machine-drive system. In this case, assume that the CEM has a fixed leakage impedance Z_l^{cm} such that a changing k will only affect the distribution of impedance in each phase leg in the MM model in order to maintain the single-phase asymmetry layout. Therefore, the leakage impedance can then be redefined as

$$Z_l^{\mathrm{cm}} \triangleq \frac{1}{3}Z_l = \frac{1}{k+2}Z_{l,\mathrm{new}} \tag{15}$$

$$Z_{l,\mathrm{new}} = \frac{k+2}{3}Z_l \tag{16}$$

where $Z_{l,\mathrm{new}}$ is the newly defined leakage impedance. After substituting the original Z_l into $Z_{l,\mathrm{new}}$ in Fig. 1, the leakage impedance at every phase leg will have the dependency of k.

Refer to the CEM in Fig. 3c, the definition of v_s^{cm} in Eq. (11) shows that the CM input voltage is dependent on the switch behavior and the dc bus voltage. The switching waveforms in v_s^{cm} introduce a high-frequency ringing in the CM current as shown by overlaying CM current i_{cm} with and without v_s^{cm} in Fig. 6. The CEM without v_s^{cm} can be considered as a dynamic average model of the CEM with v_s^{cm}. It can be concluded that except for the disappearance of high-frequency ringing, removing v_s^{cm} will not affect the machine's steady-state CM behavior.

In addition, according to Eq. (10), the mode-conversion term $v_l^{\mathrm{dm}\to\mathrm{cm}}$ is dependent on both voltage drops at DEM-AB and DEM-BC. Once v_s^{cm} has been neglected in the previous step, $v_l^{\mathrm{dm}\to\mathrm{cm}}$ then only serves as the voltage source in the CEM. Once the high-frequency components of the stator windings in Fig. 3 have been neglected, voltage division will be used to determine the voltage drop on the leakage path of DEM-AB

$$v_{l,ab}^{\mathrm{dm}} = \frac{2Z_{l,\mathrm{new}}}{2Z_f + 2Z_{l,\mathrm{new}}} \cdot \frac{\sqrt{3}}{2}V_{\mathrm{dc}} \cdot \sin\omega t \tag{17}$$

For DEM-BC, using Thévenin's Theorem to find $v_{l,bc}^{\mathrm{dm}}$ provides

$$v_{l,bc}^{\mathrm{dm}} = \frac{1}{2Z_f + \frac{6}{2k+1}Z_{l,\mathrm{new}}}\left[\frac{6}{2k+1}Z_{l,\mathrm{new}} \cdot \frac{\sqrt{3}}{2}V_{\mathrm{dc}}\sin\left(\omega t - \frac{2\pi}{3}\right) + 2Z_f \cdot v_{l,bc}^{\mathrm{cm}\to\mathrm{dm}}\right] \tag{18}$$

Although the dependent voltage source $v_{l,bc}^{\mathrm{cm}\to\mathrm{dm}}$ has dependencies on both $v_{l,ab}^{\mathrm{dm}}$ and v_l^{cm}, in most cases the DM voltages are usually two orders of magnitude greater than CM voltage. Therefore, v_l^{cm} has very limited influence on the DEM therefore can be neglected. Under this circumstance, $v_{l,bc}^{\mathrm{cm}\to\mathrm{dm}}$ in Eq. (9) can then be restated as

$$v_{l,bc}^{\mathrm{cm}\to\mathrm{dm}} \approx -\frac{k-1}{2k+1}v_{l,ab}^{\mathrm{dm}} \tag{19}$$

Substitute Formula (19) into Eq. (18), Eq. (18) then becomes

$$v_{l,bc}^{\mathrm{dm}} = \frac{1}{2Z_f + \frac{6}{2k+1}Z_{l,\mathrm{new}}} \cdot \left[\frac{6}{2k+1}Z_{l,\mathrm{new}} \cdot \frac{\sqrt{3}}{2}V_{\mathrm{dc}} \cdot \sin\left(\omega t - \frac{2\pi}{3}\right) - 2Z_f \cdot \frac{k-1}{2k+1}v_{l,ab}^{\mathrm{dm}}\right] \tag{20}$$

Finally, substitute Eqs. (17) and (20) into the $v_l^{\mathrm{dm}\to\mathrm{cm}}$ expression in Eq. (10), the approximated CM voltage source can be expressed as

$$v_{l,\mathrm{approx}}^{\mathrm{cm}} = \sqrt{2}V_{\mathrm{dc}} \cdot d(1-k) \cdot |K_f| \cdot \sin\left(\omega t - \frac{\pi}{3} + \theta_K\right) \tag{21}$$

where V_{dc} is the RMS amplitude of commanded phase voltage

$$V_{\mathrm{dc}} = \frac{1}{2} \cdot \frac{1}{\sqrt{2}}V_{\mathrm{dc}} \tag{22}$$

d is the duty cycle of the switches, and K_f and θ_K are dependent by k, which are given by

$$K_f = \frac{1}{(2k+1)\frac{Z_f}{Z_l} + k + 2} \tag{23}$$

$$\theta_K \triangleq \mathrm{Arg}\left\{K_f\right\} \tag{24}$$

The approximated CM equivalent circuit is shown in Fig. 7, where the k-dependent voltage source alone is

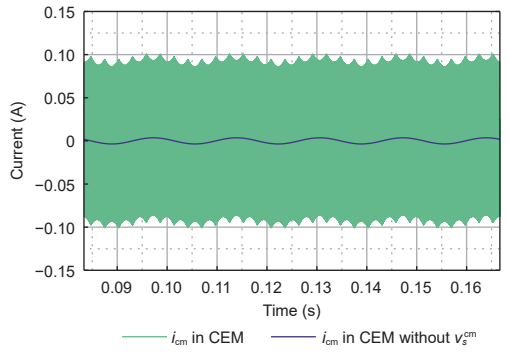

Fig. 6 CM current between CEMs with/without CM bus voltage source.

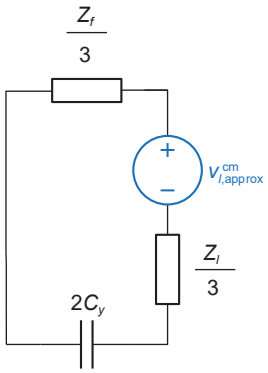

Fig. 7 CEM with dependent CM voltage source approximation.

able to determine the phase shift and amplitude change in the original CEM.

5 Discussion

Given a fixed value of k, Figs. 8 and 9 show the overlaid comparison of i_{cm} and v_{cm}, respectively. It is noticeable that the approximated voltage source is able to capture the steady-state behavior of i_{cm} with the high-frequency ringing disappearing. Hence the approximated model presented in Section 4 also serves as the dynamic average model of the original decomposed CEM at a steady state.

Comparing Figs. 3c and 7, major modifications have been made to the approximated CEM. First and foremost, the controlled voltage source in Fig. 3 relies on the behavior from the MM model, which makes the CEM not completely detached from the original machine-drive system. The direct influence of asymmetric aging at stator winding insulation is to introduce CM noise into the system, thus any

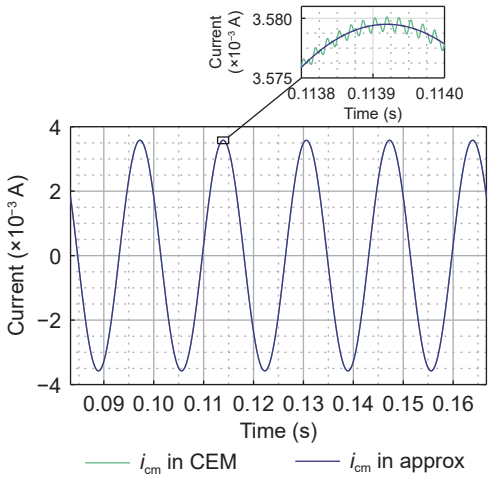

Fig. 8 CM current comparison between CEM and the approximated model.

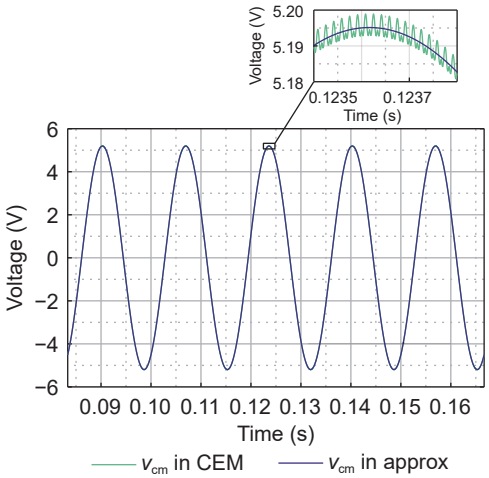

Fig. 9 CM voltage comparison between CEM and the approximated model.

turbulence from the dc bus could overwhelm the actual CM behavior from this asymmetry. Instead, the approximated source does not borrow any signals from the MM model, and all the inputs of Eq. (21) are taken only from the system setup. This eliminates the chance for unexpected system behavior to contaminate the CM noise result. Second, from Eq. (15), the CM leakage impedance is evenly distributed to each phase such that the CM impedance has no dependency on k, in another word, Z_l^{cm} is time-invariant. Having the admittance asymmetry factor lumped within the source makes the model design consistent across the entire machine lifespan. This is convenient for analyzing the aging effect beginning from the early stage of the machine operation, where all the machine parameters are characterized in a good state. Third, as stated in Section 4, the CM input voltage v_s^{cm} is neglected due to its high-frequency switching response. The CM noise has a relatively smaller magnitude compared to the DM quantity, the latter, if included, can cast a shadow over the expected CM noise, making it obscure from observation.

The observation of CM current as purposed in this method is under normal machine operation range, and this is helpful to reduce the level of CM current for accurate measurement. As for the HF content in PWM, it can cause CM current to fluctuate rapidly, making it more difficult to accurately measure or analyze the machine insulation SOH. The higher harmonic content would obscure the actual behavior from degraded insulation such that the CM profile could be unnecessarily complex. However, there are several ways to prevent HF PWM from obscuring the SOH

observation. For example, sensors or probes with higher bandwidth can be used to minimize the effects of PWM on the measurement. Some measurement and analysis techniques such as adaptive filtering algorithms are also designed to handle complex waveforms and high harmonic content. Other methods that are proven effective can be fast Fourier transform analysis and wavelet analysis. Both of the methods decompose CM waveforms into individual harmonic components or a set of wavelets, respectively, and then identify abnormalities in each component at a different scale.

Experimental validation works will be done as future work in order to better characterize and track insulation SOH. Especially for the variations in the gating signal such as HF PWM, it will largely affect the CM leakage current due to the nonlinearity of the voltage-souce inverter. Therefore, in the hardware validation stage, the nonlinearity of inverter signals will be carefully characterized and properly compensated in order to ensure the accuracy of CM leakage measurement. For the lifespan of the machine-drive system, the aging effect can typically last for years until the machine breaks down, even with asymmetric aging[4]. Compared to the stator winding insulation monitoring time, which is relatively short, the value of k can be considered constant within each monitoring interval. The approximated CM voltage source $v_{l,\text{approx}}^{\text{cm}}$ results in sinusoidal voltage and current waveforms with a fixed amplitude and phase. By setting up a proper baseline CM behavior and monitoring the SOH in a continuous manner, the insulation degradation process might be characterized with respect to the value of k. Furthermore, by understanding the k-variation trends, the approximated CEM could be used to predict the degradation rate for the next steps, thus preventive maintenance can be arranged accordingly.

6 Conclusion

This paper proposed a method for modeling and characterizing machine winding asymmetric aging effects. It is proven that without intrusive hardware installation, the machine stator windings insulation health can be monitored from the decomposed CEM. The proposed machine-drive system is modeled and then approximated using CM and DM decomposition techniques, where the final form of CEM shown in Fig. 7 is independent of the original MM model. This enables the online monitoring of the machine SOH by examining the CM system behavior. The decomposed CEM is able to fully represent the CM behavior from the MM model, after parameterization and some proper approximations, the CM current can be perceived and further predicted in a simplified RC circuit. As seen in Figs. 8 and 9, the system response due to single-phase asymmetric aging is observed with respect to a time-dependent admittance factor k. In addition, the system approximation provides insight into CM behavior changing with the winding insulation degradation process. Linking the approximated model to the insulation material SOH could provide useful information for future system preventive maintenance work.

References

[1] M. Kaufhold, G. Borner, M. Eberhardt, and J. Speck, Failure mechanism of the interturn insulation of low voltage electric machines fed by pulse-controlled inverters, *IEEE Electrical Insulation Magazine*, vol. 12, no. 5, pp. 9–16, 1996.

[2] M. Kaufhold, H. Aninger, M. Berth, J. Speck, and M. Eberhardt, Electrical stress and failure mechanism of the winding insulation in PWM-inverter-fed low-voltage induction motors, *IEEE Transactions on Industrial Electronics*, vol. 47, no. 2, pp. 396–402, 2000.

[3] N. J. Jameson, M. H. Azarian, and M. Pecht, Improved electromagnetic coil insulation health monitoring using equivalent circuit model analysis, *International Journal of Electrical Power & Energy Systems*, vol. 119, p. 105829, 2020.

[4] J. Yang, S. B. Lee, J. Yoo, S. Lee, Y. Oh, and C. Choi, A stator winding insulation condition monitoring technique for inverter-fed machines, *IEEE Transactions on Power Electronics*, vol. 22, no. 5, pp. 2026–2033, 2007.

[5] K. Younsi, P. Neti, M. Shah, J. Y. Zhou, J. Krahn, K. Weeber, and C. D. Whitefield, On-line capacitance and dissipation factor monitoring of AC stator insulation, *IEEE Transactions on Dielectrics and Electrical Insulation*, vol. 17, no. 5, pp. 1441–1452, 2010.

[6] D. Zheng, G. Lu, and P. Zhang, An improved online stator insulation monitoring method based on common-mode impedance spectrum considering the effect of aging position, *IEEE Transactions on Industry Applications*, vol. 58, no. 3, pp. 3558–3566, 2022.

[7] M. Karimi, M. Majidi, H. MirSaeedi, M. M. Arefi, and M. Oskuoee, A novel application of deep belief networks in learning partial discharge patterns for classifying corona, surface, and internal discharges, *IEEE Transactions on Industrial Electronics*, vol. 67, no. 4, pp. 3277–3287, 2019.

[8] Y. Xie, J. Zhang, F. Leonardi, A. R. Munoz, M. W. Degner, and F. Liang, Voltage stress modeling and measurement for random-wound machine windings driven by inverters, *IEEE Transactions on Industry Applications*, vol. 56, no. 4, pp. 3536–3548, 2020.

[9] F. Perisse, P. Werynski, and D. Roger, A new method for AC machine turn insulation diagnostic based on high frequency resonances, *IEEE Transactions on Dielectrics and Electrical Insulation*, vol. 14, no. 5, pp. 1308–1315, 2007.

[10] P. Nussbaumer, C. Zoeller, T. M. Wolbank, and M. A. Vogelsberger, Transient distribution of voltages in induction machine stator windings resulting from switching of power electronics, in *Proc. IECON 2013-39th Annual Conference of the IEEE Industrial Electronics Society*, Vienna, Austria, 2013, pp. 3189–3194.

[11] I. Tsyokhla, A. Griffo, and J. Wang, On-line monitoring of winding insulation health using high frequency common mode voltage from PWM, in *Proc. 2015 IEEE International Electric Machines & Drives Conference* (*IEMDC*), Coeur d'Alene, ID, USA, 2015, pp. 1433–1439.

[12] W. R. Jensen, E. G. Strangas, and S. N. Foster, Online estimation of remaining useful life of stator insulation, in *Proc. 2017 IEEE 11th International Symposium on Diagnostics for Electrical Machines, Power Electronics and Drives* (*SDEMPED*), Tinos, Greece, 2017, pp. 635–641.

[13] D. Xiang, H. Li, H. Yan, Y. Zheng, N. Zhao, and B. Liu, Online monitoring of incipient turn insulation degradation for inverter-fed machine using sensitive tail component in PWM switching oscillations, *IEEE Transactions on Power Electronics*, vol. 36, no. 8, pp. 8730–8742, 2021.

[14] G. Zanuso and L. Peretti, Evaluation of high-frequency current ringing measurements for insulation health monitoring in electrical machines, *IEEE Transactions on Energy Conversion*, vol. 37, no. 4, pp. 2637–2644, 2022.

[15] H. Li, Y. Gu, D. Xiang, P. Zhang, P. Yue, and Y. Cui, Online condition monitoring of line-end coil insulation for inverter-fed machine by switching oscillation mode decomposition, *IEEE Transactions on Industrial Electronics*, vol. 69, no. 11, pp. 11697–11708, 2021.

[16] F. Niu, Y. Wang, S. Huang, L. Wu, X. Huang, Y. Fang, and T. Yang, An online groundwall insulation monitoring method based on transient characteristics of leakage current for inverter-fed motors, *IEEE Transactions on Power Electronics*, vol. 37, no. 8, pp. 9745–9753, 2022.

[17] J. E. Antón, J. M. Guerrero, and C. A. Platero, A frequency response analysis and machine learning combined method for interturn faults identification in synchronous generators, in *Proc. 2021 IEEE International Conference on Environment and Electrical Engineering and 2021 IEEE Industrial and Commercial Power Systems Europe* (*EEEIC/ I&CPS Europe*), Bari, Italy, 2021, pp. 1–6.

[18] Z. Zhao, Y. Chen, Y. Yu, M. Han, C. Tang, and C. Yao, Equivalent broadband electrical circuit of synchronous machine winding for frequency response analysis based on gray box model, *IEEE Transactions on Energy Conversion*, vol. 36, no. 4, pp. 3512–3521, 2021.

[19] F. Babaa, O. Bennis, F. Kratz, and A. Hadri-Hamida, Combined electrical faults detection and diagnosis using current signature analysis, in *Proc. 2021 IEEE 13th International Symposium on Diagnostics for Electrical Machines, Power Electronics and Drives* (*SDEMPED*), Dallas, TX, USA, 2021, pp. 52–57.

[20] K. K. Swarnkar, J. Rai, and S. Wadhwani, Stator inter-turn fault diagnosis by motor current signature approach, in *Proc. 2022 4th International Conference on Smart Systems and Inventive Technology* (*ICSSIT*), Tirunelveli, India, 2022, pp. 584–588.

[21] H. W. Penrose, Evaluation of asynchronous wind generator stator magnetic slot wedge and coil movement using electrical signature analysis, in *Proc. 2021 IEEE Electrical Insulation Conference* (*EIC*), Denver, CO, USA, 2021, pp. 1–4.

[22] P. Nussbaumer, M. Vogelsberger, and T. Wolbak, Induction machine insulation health state monitoring based on online switching transient exploitation, *IEEE Transactions on Industrial Electronics*, vol. 62, no. 3, pp. 1835–1845, 2015.

[23] P. Zhang, K. Younsi, and P. Neti, A novel online stator ground-wall insulation monitoring scheme for inverter-fed AC motors, in *Proc. 2013 IEEE Energy Conversion Congress and Exposition*, Denver, CO, USA, 2013, pp. 3541–3547.

[24] F. Hassani, N. H. Faisal, R. Nish, S. Rothnie, and J. Njuguna, The impact of thermal ageing on sealing performance of HNBR packing elements in downhole installations in oilfield wellhead applications, *Journal of Petroleum Science and Engineering*, vol. 208, p. 109200, 2022.

[25] S. B. Lee and J. Yang, An on-line groundwall and phase to phase insulation quality assessment technique for AC machine stator windings, in *Proc. 2005 40th Industry Applications Conference*, Hong Kong, China, 2005, pp. 10–19.

[26] A. Brovont, Generalized differential-common-mode decomposition for modeling conducted emissions in asymmetric power electronic systems, *IEEE Transactions on Power Electronics*, vol. 33, no. 8, pp. 6461–6466, 2018.

[27] J. Jatskevich and O. Wasynczuk, Automated state model generator, https://pcka.com/?page_id=80, 2023.

[28] L. Wang, C. N. -M. Ho, F. Canales, and J. Jatskevich, High-frequency modeling of the long-cable-fed induction motor drive system using TLM approach for predicting overvoltage transients, *IEEE Transactions on Power Electronics*, vol. 25, no. 10, pp. 2653–2664, 2010.

[29] B. Wang, J. Wang, A. Griffo, A. I. Patel, Z. Sun, E. Chong, and R. Smitham, Permanent magnet generator turn fault detection using kalman filter technique, in *Proc. 2016 IEEE Energy Conversion Congress and Exposition* (*ECCE*), Milwaukee, WI, USA, 2016, pp. 1–8.

[30] A. Bellini, F. Filippetti, C. Tassoni, and G. -A. Capolino, Advances in diagnostic techniques for induction machines, *IEEE Transactions on Industrial Electronics*, vol. 55, no. 12, pp. 4109–4126, 2008.

[31] S. Ogasawara and H. Akagi, Modeling and damping of high-frequency leakage currents in PWM inverter-fed AC motor drive systems, *IEEE Transactions on Industry Applications*, vol. 32, no. 5, pp. 1105–1114, 1996.

Aaron D. Brovont received the BS degree in electrical engineering, the MS degree in electrical and computer engineering, and the PhD degree from Purdue University, West Lafayette, IN, USA in 2011, 2013, and 2016, respectively. From 2016 to 2019, he served as an assistant professor of electrical and computer engineering at The University of Alabama, specializing in the modeling and simulation of electromechanical systems and electromagnetic compatibility of power electronic systems. In 2019, he joined PC Krause and Associates, as a senior lead engineer. He is a member of IEEE. His research interests include modeling and design of power electronic systems for optimal EMI mitigation, utilization of common-mode behavior for power system monitoring and control, and numerical methods for use with population-based design of power system components.

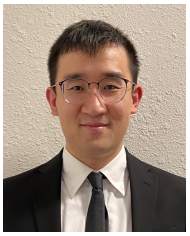

Jin Zhao received the BS degree in industrial engineering from Beijing University of Chemical Technology in 2012, and the MS degree in electrical engineering from SUNY University at Buffalo in 2014. He is currently pursuing the PhD degree in electrical and computer engineering at The University of Alabama with a concentration in battery behavioral modeling and characterization. His research topics of interest include modeling and simulation on complex systems, data analysis, battery management systems, etc.